CONFERENCE PRE-PRINT

SIMULATION OF STOCHASTIC TRANSPORT AND DEPOSITION OF SEED RUNAWAY ELECTRONS DURING ITER SPI

Y.X. Sun, D. Hu, B. Li, Y. Yuan, L. Cheng, Y.H. Li
Beihang University
Beijing, China
Email: hudi2@buaa.edu.cn

F. Wang
Dalian University of Technology
Dalian, China

A.N. the JOREK team
See Hoelzl et al 2024 (https://doi.org/10.1088/1741-4326/ad5a21)

Abstract

Runaway electrons (REs) during the Current Quench can significantly impact the operational limits and component lifetime of future high-performance tokamaks such as ITER. Localized, uncontrolled RE deposition can cause severe damage to first-wall surfaces and structural components. This risk is particularly serious if REs replace bulk electrons as the main current carrier. One way to avoid such current replacement is to deplete the seed REs within the plasma through stochastic trajectory loss before they have time to avalanche. To investigate such stochastic transport behavior as part of the ITER disruption mitigation scheme, the researchers carry out guiding center simulations of the seed REs with a conservative higher-order magnetic moment using the PTC code based on fluid fields produced by JOREK simulations. Focusing on an ITER plasma after Shattered Pellet Injection, which experiences breaking-up and healing of flux surfaces, the REs transport properties are investigated. Self-similar density profile and exponential decay of seed REs are found for case with sufficiently stochastic magnetic field. The timescale of seed REs loss is compared with the avalanche time to estimate the efficiency of stochastic REs depletion during the mitigation process. Using a realistic 2D wall, the seed REs' hit map shows a pattern with a dominant n=1 mode along with higher-order harmonics. Finally, the diffusion transport coefficient of seed REs is obtained statistically through the simulations and compared with the particle radial flux, and used to solve the radial diffusion equation to get a density profile that similar to the profile from simulation. The study may provide valuable insights for optimizing mitigation techniques and protecting plasma-facing components from localized RE impacts.

1. INTRODUCTION

Runaway electrons (REs) can significantly impact the operational limits and component lifetime of future high-performance tokamaks such as ITER due to their potential to cause severe damage to plasma-facing components (PFCs). During plasma disruptions, REs can be generated and multiply via the avalanche mechanism, potentially causing severe damage to plasma-facing components once they deposit on the first wall. One way of preventing such an RE avalanche is to induce enhanced RE transport. If the characteristic RE loss time or scattering time is smaller than the avalanche time, then the seed REs will leave the system before they can undergo multiplication. An especially interesting scenario of such enhanced loss is the RE transport during the Thermal Quench (TQ) or its mitigation via disruption mitigation systems such as Shattered Pellet Injection (SPI). It is desirable to deplete most of the seed REs within the plasma before significant avalanche occurs to help the RE current mitigation during the following Current Quench (CQ) phase.

To illustrate the dominant RE transport behavior at the stage of TQ mitigation, we investigate seed REs transport using the particle tracing code (PTC) [1] with high-order conservative magnetic moment [2]. The simulations are based on fluid fields produced by JOREK MHD simulations [3], which models the stochastic magnetic configurations during disruption mitigation. Our analysis reveals that a transport eigen solution like behavior emerges during the depletion process. The RE loss time is found to be much smaller compared to the MHD evolution time, and the RE transport flux could be well described by a diffusive model when the field lines are sufficiently stochastic. The statistical transport coefficient is found to be generally in agreement with previous quasilinear analytical results.

2. NUMERICAL METHODS AND BACKGROUND FIELDS

This work is mainly based on a test particle tracing code named PTC, which is capable of both full orbit and drift orbit solvers [1]. The code has been upgraded to extract the gradient and curvature from JOREK fields, which allows for the full utilization of high-order conservative magnetic moment modification [2]. It should be noted that the equations of motion are solved using the 4th order Runge-Kutta method (RK4) in the code, which does not exactly preserve energy. Therefore, the time step is carefully chosen to ensure that the error remains sufficiently small. In the study, we initialized 1×10^5 particles with a 5 MeV energy in the plasma region, and the pitch angle $(p_\parallel/p_{total})$ is set to 0.9.

2.1. High order conservative magnetic moment

The guiding-center solver is used in this work for its efficiency over the full orbit solver. An especial concern regarding RE particle simulations is the accuracy of the guiding center approximation for highly relativistic energy range. Traditional guiding-center theory assumes the conservation of the magnetic moment ($\mu = p_\perp^2/2mB$), but full-orbit simulations have shown that this assumption breaks down for REs with higher energy, depending on the pitch angle [4]. Recent work by Liu et al [2] has addressed this issue by deriving a higher order expression for the magnetic moment that significantly improves its conservation even for highly relativistic REs. The magnetic moment can be expanded to the second order as:

$$\mu = \frac{\left| p_\perp + p_\parallel^2 \boldsymbol{\kappa} \times \frac{\boldsymbol{b}}{qB} \right|^2}{2m_0 B} = \mu_0 + \mu_1 + \mu_2, \tag{1}$$

$$\mu_0 = \frac{p_\perp^2}{2m_0 B}, \quad \mu_1 = \frac{p_\parallel^2 p_\perp \cdot \boldsymbol{\kappa} \times b}{q m_0 B^2}, \quad \mu_2 = \frac{p_\parallel^4}{q^2 B^2} \frac{|\boldsymbol{\kappa} \times b|^2}{2m_0 B}, \tag{2}$$

where $\boldsymbol{\kappa}$ is the curvature vector of the magnetic field-line defined by $\boldsymbol{\kappa} = (\boldsymbol{b} \cdot \boldsymbol{\nabla})\boldsymbol{b}$ with $b = B/B$, $\boldsymbol{p}_\perp = \boldsymbol{b} \times (\boldsymbol{p} \times \boldsymbol{b})$, $p_\parallel = \boldsymbol{p} \cdot \boldsymbol{b}$ is the parallel kinetic momentum, m_0 is the rest mass of the particle.

2.2. Stochastic background field

Particle simulations by PTC are carried out based on static fluid fields produced in previous JOREK [5] mitigated TQ simulations for ITER. The perturbed magnetic energies throughout the SPI process are shown in FIG. 1 (*a*), and the *n*=1 component of the magnetic energy should be focused on, which is plotted as the orange line, since it is the dominant component. The chosen time slice is marked by the red vertical dashed line. The Poincare plot of the magnetic field shown in FIG. 1 (*b*). and the stochasticity is clearly visible from the plot. The colors of the Poincare point represent different initial position of the field line tracers.

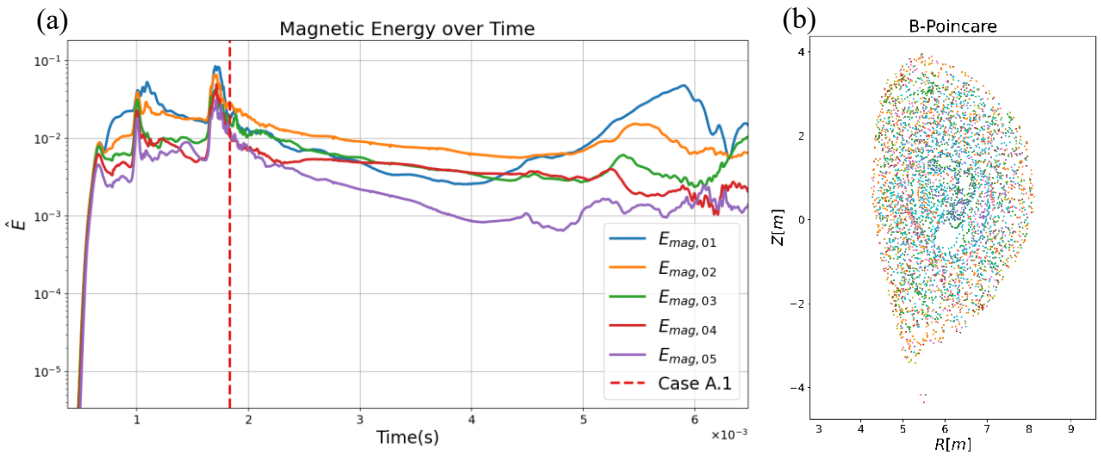

FIG. 1. Magnetic energy and Poincare of the background fluid field.

3. SELF-SIMILAR RES DENSITY PROFILE

The normalized density profiles of REs in stochastic fields exhibit self-similarity regardless of initial distribution, as shown in FIG. 2. The density profiles are normalized by the total number of particles remaining in the simulation domain at each time. The X-axis represents the normalized poloidal flux $\hat{\psi} = (\psi - \psi_{axis})/(\psi_{bnd} - \psi_{axis})$. Two initial REs density profiles are chosen: one peaked and one flat, represented by the blue and red shade solid lines respectively. The red curves ("RZ") correspond to particles uniformly initialized in the poloidal plane, resulting in a flat distribution profile. In contrast, the blue curves ("OMP") represent particles initialized uniformly in the Outer Mid-Plane (OMP). Due to the small plasma volume near the magnetic axis, the particle density is higher in this region, leading to a peaked distribution. The dashed lines show the distribution after a short time, and the dash-dotted lines indicate the self-similar density profile reached. The evolutions of each initial profile are shown in different color tones (blue for peaked and red for flat), with the simulation time indicated on the label.

From this figure, we can see the red and blue dash-dotted lines are almost identical apart from a small region near the axis, which means both initial schemes will converge to the same self-similar density profile within $50\ \mu s$, whereas the background field evolves on a timescale almost one order of magnitude longer (see FIG. 1 (a)). Hence there exists a timescale separation between the time needed for the REs to reach the self-similar profile and the time of magnetic field evolution. Such relatively slow magnetic field evolution justifies our choice of using static field as the background magnetic field in our simulation.

Apart from the self-similar spatial density profile, the time evolution of RE transport also exhibit clear exponential form, as shown in FIG. 3 (a). This figure shows the distribution of lost particles over time. The red solid line is the exponential fitting of the lost particles, and FIG. 3 (a) matches the exponential decay well. Such exponential decay of RE population in a strongly stochastic magnetic field has been reported previously by Papp et al [6].

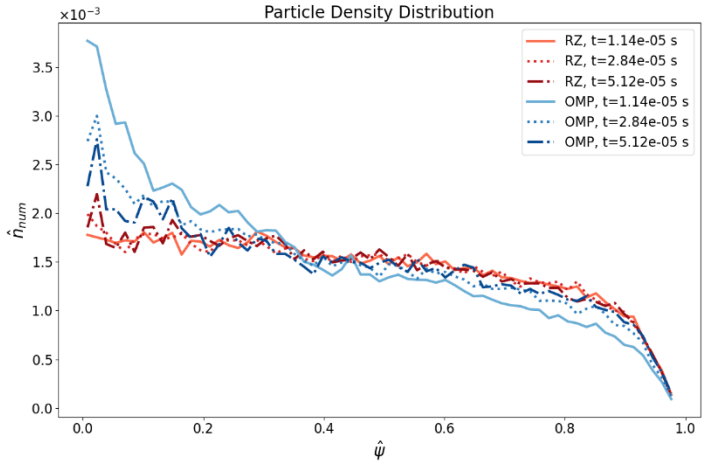

FIG. 2. The normalized density profile of REs in stochastic field with different initial distribution.

For the radial diffusion equation:

$$\frac{\partial n}{\partial t} = \frac{1}{r}\frac{\partial}{\partial r}\left(rD(r)\frac{\partial n}{\partial r}\right), \tag{3}$$

we solve it by using diffusion coefficients obtained from simulation via the method introduced by Särkimäki et al. [7] (discuss in SEC. 5.1). The left hand of this equation can rewrite as $\partial n/\partial t = \lambda n, \lambda = -1/\tau$, τ is the characteristic loss time (discuss in SEC. 4). The first-order eigenmode density n is normalized following the same procedure as in Fig. 2. A comparison between the normalized density profile from particle simulation and the eigenmode solution is presented in Fig. 3 (b). The close agreement between the two profiles suggests the existence of the eigen-solution.

The self-similar normalized density profile is not only independent of initial distribution but also of initial pitch angle and energy, so long as the trapped population is small, as shown in FIG. 4.

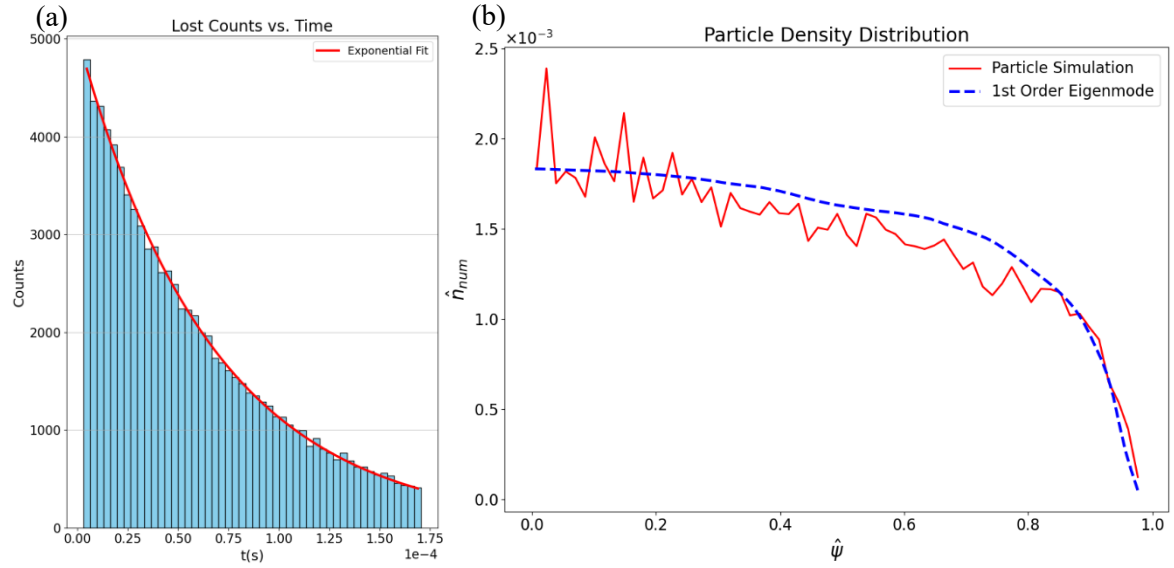

FIG. 3. Distributions of lost particles over time and Comparison of eigenmode density profile.

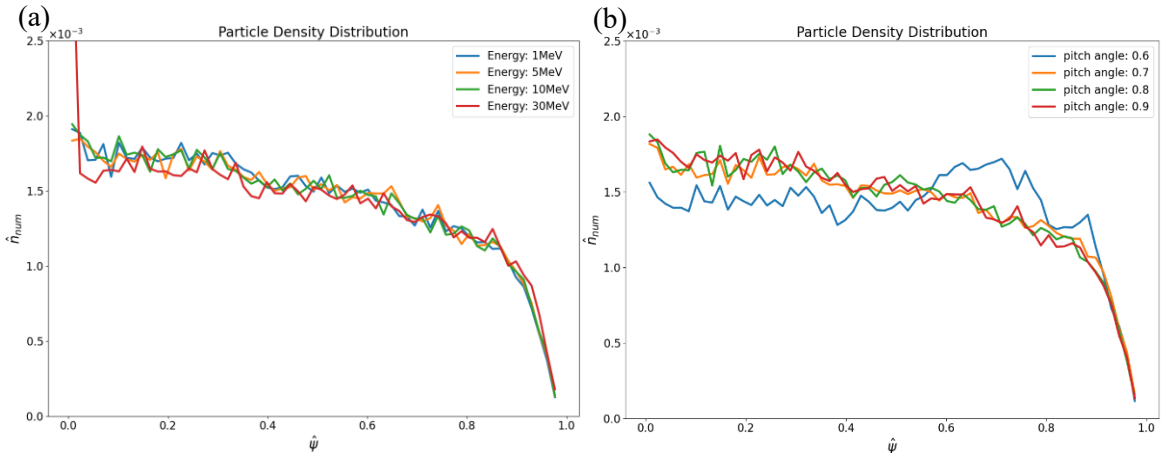

FIG. 4. The self-similar normalized density profile of REs with different (a) initial energies and (b) pitch angles.

In FIG. 4 (*a*), although particles with initial energy of 30 MeV near the magnetic axis are less influenced by the stochastic magnetic field compared to other particles, the normalized density profiles still exhibit self-similarity. In FIG. 4 (*b*), the normalized density profiles for pitch angles from 0.7 to 0.9 are nearly identical, while the profile for a pitch angle of 0.6 deviates due to the different behavior of trapped particles compared to passing particles. The resulting profiles consistently exhibited self-similarity, confirming the robustness of our findings.

4. RE LOSS TIMESCALE AND DISTRIBUTION

Another issue of interest is the deposition of the REs lost onto the first wall or the divertor targets. During the PTC simulation, we can record the positions and times when particles get lost. As previously shown in FIG. 3 (*a*), we observed that the number of lost particles over time closely follows an exponential curve, with a determination coefficient $R^2 = 0.997$. The rate of loss of REs can be represented by the following equation:

$$N_{\text{loss}}(t) = -\frac{\mathrm{d}N_{\text{plasma}}(t)}{\mathrm{d}t} = \frac{1}{\tau} \cdot N_0 \cdot e^{-\frac{t}{\tau}}. \tag{4}$$

The reciprocal of exponent part τ is 6.63×10^{-5} s. We use this value as the characteristic loss time for this field. To overcome the avalanche process of REs, the loss time should be shorter than $1 - 10$ ms [36], which is much longer than the characteristic loss time we obtained. This indicates that the stochastic field is effective in suppressing the avalanche process of REs.

FIG. 5 (a) shows the poloidal plane projection of the REs' lost position with red dots. As can be seen, even for complete stochastic magnetic field lines, REs in our simulation still dominantly deposits on the divertor region. The in-out asymmetry of the divertor deposition is caused by the helicity of the magnetic field lines and the directional velocity of the REs.

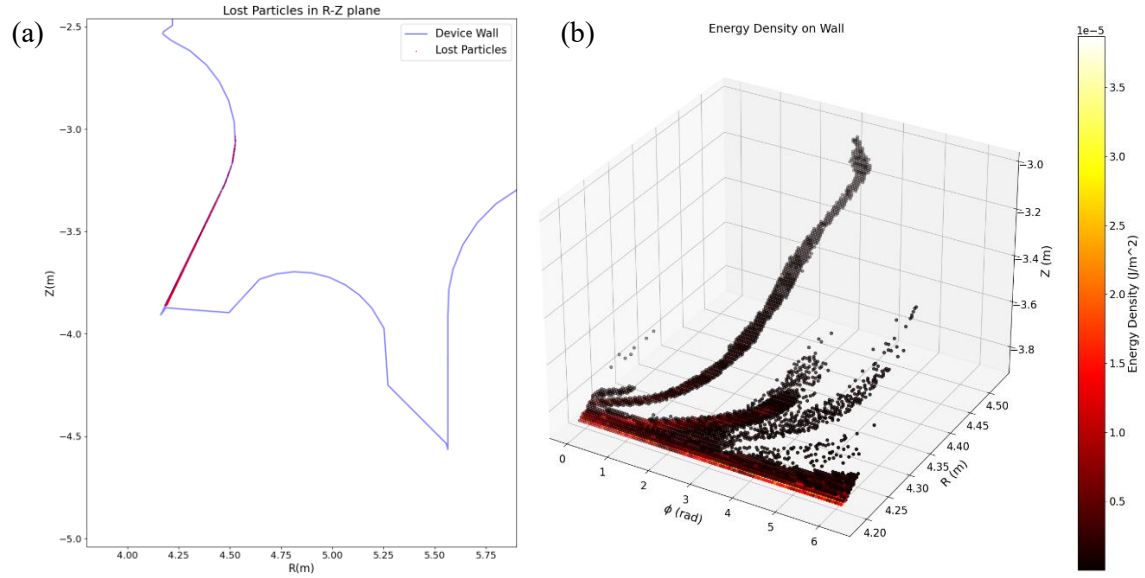

FIG. 5. Lost Position and Heatmap of Lost Energy.

FIG. 5 (b) presents the heat map of the cumulative energy deposited on the wall by lost REs, with the distribution unwrapped toroidally to reveal the deposition pattern. The pattern shows that the majority of particles strike the bottom poloidal belt, which exhibits a much higher energy density. In contrast, the upper region features the dominant n=1 mode and higher-order harmonics. This structure indicates that the lost REs followed specific magnetic field lines from the plasma core, through the scrape-off layer, to the first wall. It is crucial to note that the color bar values are relative and reflect the deposition pattern under these specific simulation conditions; they do not represent absolute physical energy scales.

5. TRANSPORT COEFFICIENT

5.1. Transport coefficient evaluation theory

The transport coefficients, advection V and diffusion D, have been widely used to describe the stochastic transport of REs. The transport coefficients can be derived from numerical results using the method proposed by Särkimäki et al [7], which we briefly reviewed here.

If the initial distribution of particles is represented by a Dirac delta function as $f(r,0) = \delta(r_0 - r)$, then it would evolve as a Gaussian function:

$$f(r,\tau) = \frac{1}{\sqrt{4\pi D_{r_0}\tau}} \exp\left[-\frac{(r - r_0 - V_{r_0}\tau)^2}{4D_{r_0}\tau}\right]. \tag{5}$$

And the transport coefficients are given in a straightforward way:

$$V_{r_0} = \frac{\mu_r - r_0}{\tau}, \qquad D_{r_0} = \frac{\sigma_r^2}{2\tau}, \tag{6}$$

where μ_r is the mean reduced minor radius of all particles start from r_0, and $\sigma_r^2 = Var(r - r_0)$ is the variance.

In order to capture the characteristics of the transport coefficients in a stochastic field, we count the particles after they pass through a specific poloidal plane over a certain time. The τ is the average time interval those particles take between subsequent passings, and μ_r, σ_r^2 can be calculated by the change of particles reduced minor radius.

Using equation (6) for computations, scanning the r_0 through the minor radius of the plasma, the advection V and diffusion D profiles can be subsequently obtained.

For fields with high stochasticity, particle transport is primarily governed by diffusion, with advection effects being negligible in comparison. Therefore, this study focuses on the diffusion coefficient D, while the advection coefficient V is not considered in the subsequent analysis.

5.2. Comparison of particle flux and diffusive flux

How well the diffusion coefficients could be used to describe the RE transport is tested by considering the diffusive particle flux $\Gamma = -D\nabla n$. From PTC outputs, we can obtain the position of every particle at each time step, so the real particle flux Γ can be calculated by the number of particles passing through a given flux surface ψ, which is corresponding to a reduced minor radius $r = r_a\sqrt{\hat{\psi}}$, in a certain time by linear interpolation. The particle density gradient ∇n is extracted from the numerical density profile, multiplying D by $-D\nabla n$ yields the diffusive flux. The comparison is shown in FIG. 6.

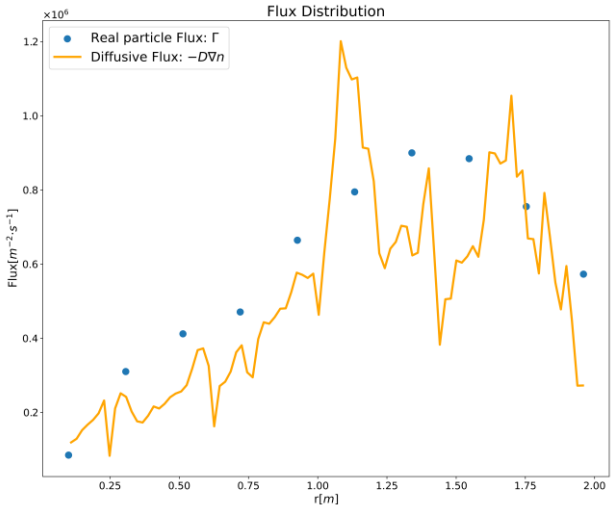

FIG. 6. Comparison of Γ(blue) and $-D\nabla n$(orange) along the reduced minor radius r.

We observed that both the RE particle flux and the diffusive flux exhibit similar magnitudes and tendencies, although their specific values do not exactly match. One reason for this discrepancy could be that the time and space resolution of the particle flux statistics are much coarser compared with that of the diffusion coefficient statistics. Such agreement between the real RE flux and the diffusive flux suggests that diffusion alone is already a good enough description of the RE transport, at least in cases with sufficiently stochastic magnetic field.

5.3. Comparison with Rechester–Rosenbluth diffusion coefficient

For the REs with relativistic speed, the collision frequency is low and the mean free path is long, which means the REs can be considered to be in a collisionless regime. In this case, the transportation can be described with the Rechester-Rosenbluth (RR) diffusion coefficient [8]:

$$D_{RR} \sim v_{\parallel} L_0 \langle b^2 \rangle. \tag{7}$$

Here $v_{\parallel} \backsimeq c$ is the parallel velocity of electrons along the magnetic field direction, $L_0 \backsimeq qR$ is the auto-correlation length of the magnetic field, and $\langle b^2 \rangle = (\delta B/B)^2$ is the mean square of the local magnetic field perturbation which can be calculated by pure fluid simulation. We hereby compare the aforementioned analytical result with our numerical one, as shown in FIG. 7. D_{num} is calculated by Eq. (5) with simulation results and D_{RR} is calculated by Eq. (7). Both of them are normalized by their maximum values. This is equivalent to choosing a constant autocorrelation length $L_0 = R$ to fit the RR result and our statistical result.

As shown in FIG. 7, the two curves exhibit similar trends. Their fluctuations are quite similar, but the maximum positions are slightly offset. The maximum unnormalized values of D_{num} and D_{RR} are $4.7067 \times 10^4\ \mathrm{m^2 s^{-1}}$

and $8.0752 \times 10^4\ \mathrm{m^2 s^{-1}}$. Although their exact magnitudes differ, they remain within the same order of magnitude, with a relative difference of less than a factor of two. One possible reason for this discrepancy is that we roughly assumed a constant auto-correlation length $L_0 = R$ in the RR formula, while in reality this parameter might depend on the magnetic perturbation. Hence our comparison here should be considered as an order of magnitude estimation. A more detailed model for the auto-correlation length is planned to be used in our future works for more meaningful comparison with analytical models.

Another explanation for the discrepancy is that the RR formula is a simplified model that doesn't capture the detailed particle behavior, whereas the numerical diffusion coefficient directly reflects the particles' trajectories. First, at relativistic speeds, electron orbit deviations from flux surfaces cause diffusion patterns that differ from RR estimations. Second, the Finite Orbit Width effect reduces the diffusion coefficient by a scaling factor Υ ($\Upsilon < 1$) applied to D_{RR}. Additionally, in open chaotic magnetic fields as used here, particles tend to be lost in the outer region before achieving full ergodicity comparable to magnetic field lines, resulting in a lower observed diffusion coefficient [6].

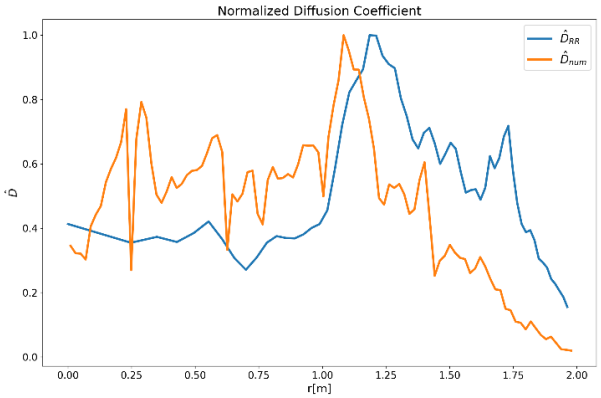

FIG. 7. Comparison of normalized numerical diffusion coefficient $\widehat{D}_{\mathrm{num}}$ and the RR diffusion coefficient $\widehat{D}_{RR}$.

6. CONCLUSION

In the study, we have investigated the transport and deposition behavior of seed REs in stochastic magnetic fields during the tokamak disruption mitigation process, by using the PTC with high-order conservative magnetic moment formulation and based on fluid fields from JOREK MHD simulations.

Our simulations reveal several key findings. The normalized density profiles of REs in stochastic fields exhibit self-similarity regardless of initial distribution, energy, or pitch angle (for passing particles). This self-similarity emerges within tens of microseconds, substantially faster than the field evolution timescale, allowing us to use static field snapshots for transport studies. This density profile also matches the eigen-solution of diffusion equation, which suggests the presence of eigenmodes of transport within the stochastic fields.

Another observation is the loss REs in fully stochastic fields follows an exponential decay pattern, which is directly responsible for the observed self-similar density profiles. The characteristic loss time is on the order of microseconds, significantly shorter than the avalanche timescale of $1 - 10$ ms, indicatingthe effectiveness of suppressing the avalanche process of REs. While most of REs hit the inner divertor, the deposition pattern shows a dominant n=1 mode along with higher-order harmonics, which indicates the REs are following certain magnetic lines to escape from the plasma region.

Our transport coefficient analysis confirms that diffusion is the dominant transport mechanism in fully stochastic regions, with good agreement between the real RE particle flux and the diffusion-driven flux. Comparison with the analytical RR diffusion model shows similar trends but quantitative differences, particularly in the outer plasma regions where orbit effects and particle losses become significant.

Understanding the transport and deposition patterns offers valuable insights for optimizing mitigation techniques and protecting plasma-facing components from localized RE impacts. Future work will focus on calculating the

transport coefficients from the numerical results and further analyzing them to enhance the robustness of these findings, as well as including the radiative drag and collision effect.

ACKNOWLEDGEMENTS

The authors thank C. Liu, L. Wang and Y.P. Zhang for fruitful discussions. This work is supported by the National MCF Energy R&D Program of China under Grant No. 2024YFE03230100 and the National MCF Energy R&D Program of China under Grant No. 2019YFE03010001. This work is carried out partly on Tianhe-3 operated by NSCC-TJ.

REFERENCES

[1] F. Wang, et al, PTC: Full and Drift Particle Orbit Tracing Code for α Particles in Tokamak Plasmas, Chinese Phys. Lett. **38** 5 (2021) 055201.

[2] C. Liu, et al, Conservative magnetic moment of runaway electrons and collisionless pitch-angle scattering, Nucl. Fusion **58** 10 (2018) 106018.

[3] M. Hoelzl, et al, Non-linear MHD modelling of transients in tokamaks: a review of recent advances with the JOREK code, Nucl. Fusion **64** (2024) 112016.

[4] J. Liu, et al, Collisionless pitch-angle scattering of runaway electrons, Nucl. Fusion **56** (2016) 064002.

[5] D. Hu, et al, Plasmoid drift and first wall heat deposition during ITER H-mode dual-SPIs in JOREK simulations, Nucl. Fusion **64** (2024) 086005.

[6] G. Papp, et al, Energetic electron transport in the presence of magnetic perturbations in magnetically confined plasmas, Journal of Plasma Physics, **81** (2015) 475810503.

[7] K. Särkimäki, et al, Confinement of passing and trapped runaway electrons in the simulation of an ITER current quench, Nucl. Fusion, **62** (2022) 086033.

[8] A.B Rechester. and M.N. Rosenbluth, Electron Heat Transport in a Tokamak with Destroyed Magnetic Surfaces, Phys. Rev. Lett. **40** (1978) 38.